International Journal of Robotics and Control Systems
Vol. 6, No. 1, 2026, pp. 305-323
ISSN 2775-2658
http://pubs2.ascee.org/index.php/ijrcs

Amelioration of Traditional PI Boost Converter Utilizing Linear Active Disturbance Rejection Controller - Mode Predictive Control Strategy

Saif Talal Bahar [a,1], Hao Qiu [b,2,*]

[a] Department of Electromechanical Techniques, Baquba Technical College, Middle Technical University, Baghdad, Iraq
[b] School of Mechanical and Electrical Engineering, Guilin University of Electronic Technology, Guilin, China
[1] saif.talal@mtu.edu.iq; [2] haoqiu@guet.edu.cn;
* Corresponding Author

ARTICLE INFO

Article history
Received November 12, 2025
Revised December 27, 2025
Accepted January 29, 2026

Keywords
Boost Converter;
Model Predictive Control;
LADRC-MPC;
DC-DC Converters

ABSTRACT

For a typical Boost converter, the entire control loop must be designed with a compensator to improve the circuit's dynamic and static performance. To solve the problems of conventional loop PI control of the boost converter including input current distortion, fast dynamic response, and high power. An optimization Linear Active Disturbance Rejection Controller (LADRC) algorithm is proposed, created on predictive voltage inner loop control. The algorithm solved the problems of slow dynamic response and waveform distortion of loop PI control. By simulation in MATLAB, the response curve demonstrates that, in addition to overshooting during the boosting procedure, the Boost converter with LADRC-MPC has a modification time of 22ms as opposed to 80ms with PI-MPC. While utilizing the LADRC-MPC control technique, the current time for modification is 12ms, and while using PI-MPC, it is 27ms. The simulation results indicate that the mechanism scheme created on LADRC-MPC exhibits good stability and rapidity, as well as high robustness.

1. Introduction

With the growing adoption of power electronics technology, DC-DC converters are used in both civilian and military applications. In many practical applications, a stable output voltage is required. This also raises the requirements for switching power supplies. Switching power supplies based on boost converters has become increasingly well-known to the public. Boost converter circuit topology has become the first choice for studying voltage regulation. Any circuit cannot be separated from the power supply. Therefore, studying the closed-loop control design of boost converters has significant implications and value as a reference [1], [2]. Switching converters are time-varying systems with closed-loop control, which require small-signal modeling and well-designed controllers to achieve voltage regulation requirements [3], [4]. In recent decades, the modeling and control of switching converters have been the focus of research by scholars worldwide. Given the widespread use of boost converters, it is urgent to design their control-loop compensation networks to enhance system stability and dynamic response. Different compensation networks give switching power supplies different performances. Common compensators include PD, PI, and PID compensators. The PID compensator

combines the advantages of the PD compensator and PI compensator and has become a common choice [5], [6]. Boost converters are widely used in photovoltaic systems, energy storage systems, electric vehicles, and other fields because they transfer power from low-voltage DC power supplies to high-voltage electronic loads [7], [8]. The most traditional control method uses a PI controller based on pulse width modulation (PWM) to determine the PI parameter values based on the established system average model. The standard average model usually ignores the influence of switching frequency, leading to poor dynamic performance in the control system.

In recent years, in the field of power electronic converters, model predictive control, as an industrialized mechanism theory, has the benefits of fast dynamic response, avoiding adjustment of system parameters, and increasing control system constraints compared to traditional control methods, and has therefore attracted the research of many scholars [9]. All proposed a finite-control-set model predictive control (FCS-MPC) method for inverters [10], [11]. The MPC method based on finite control sets is systematically compared with PI control, which has played an important role in promoting MPC research [12]. Applied model predictive control to boost converters and proposed different control methods [13]. Since the Boost converter is a non-minimum-phase system, a longer prediction step is required in direct voltage control, which greatly increases the computational burden of the control system. The continuous control set model is an MPC method for current. This control method assumes that the inductor current and output voltage increments continue unchanged within a sampling period. It predicts the current value at the next moment by predicting the slope of the inductor current waveform. However, this method has two main disadvantages: 1) The inductor resistance value is not considered in calculating the slope of the inductor current, resulting in inaccurate prediction results; 2) Additional sensors are required to measure the input voltage, which increases the system cost. Have proposed system disturbance observers suitable for MPC to address parameter mismatches in the system model. Still, they are too complex and increase the computational burden [14]-[16]. The priceless gifts outlined in the projected item's foundation are many and multifaceted, including a roomy range of judgments and suggestions poised to considerably advance the existing methodical study of part of the material world in the appropriate field of study.

This paper presents the occupied law of DC-DC converters and connects the LADRC-MPC control invention to design an upgraded boss. The Boost preacher, a usual DC-DC preacher, is handled as the research object in this paper. As a typical boost converter, it exhibits nonlinear dynamic characteristics. First, the topology, working mode, and operating principle of the boost circuit are introduced, along with the parameter calculation method and the steps for each component in the circuit. Secondly, an enhanced algorithm is designed to control the Boost circuit using the LADRC-MPC algorithm. The algorithm solved the problems of slow dynamic response and waveform distortion of loop PI control. The simulation results indicate that the proposed methodology exhibits commendable stability. Using the MATLAB platform, the functional implementations of the traditional PI-MPC and LADRC-MPC control algorithms were compared. Through continuous correction and calibration, simulation results confirmed that the process control effect using the LADRC-MPC algorithm is superior. The system processes of these three controllers are simulated using MATLAB Simulink modularization. Then, the dynamic response process under both the static working state and the disturbed state is compared. The enhanced algorithm LADRC-MPC has good stability and speed, as well as high robustness.

2. Method

2.1. Working Principle of Boost Converter

The boost converter, also identified as a step-up converter, is a DC converter that makes the output voltage Vo superior to the input voltage V_{in}. The circuit structure is illustrated in Fig. 1. The reason why the boost converter can make the output voltage value larger than the input voltage value is mainly because (1) the inductor L has the function of increasing the output voltage after storing energy; (2) when the diode D is turned off by reverse voltage, the capacitor C can release energy to

uphold the output voltage. Since the boost converter has a humble circuit construction and great stability, it is widely used in various portable electronic devices daily [17].

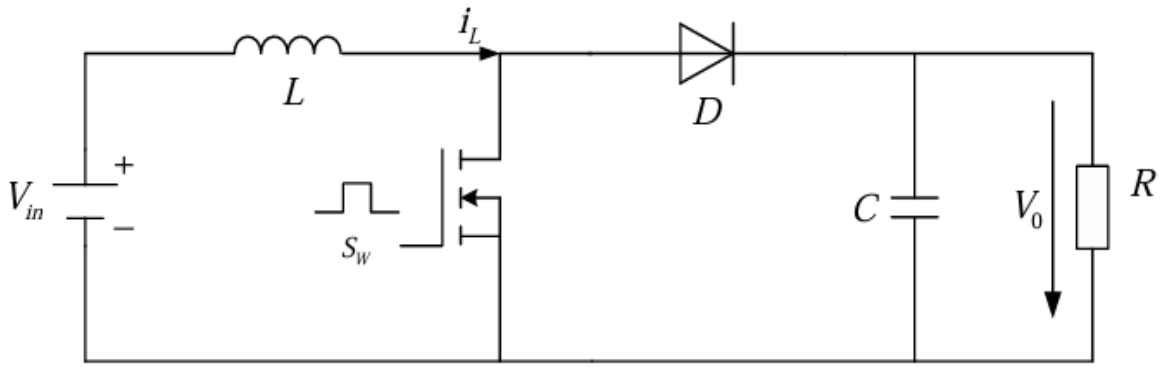

Fig. 1. Boost converter main circuit structure

In Fig. 1, Vin is the DC voltage source, L is the boost inductor, Saw is the power switch, D is the diode, C is the capacitor, and R_L is the burden resistor. i_L is the inductor current, Vo is the output voltage, and d is the controller input, which is the duty cycle of the switch Sw and satisfies d ϵ [0,1]. During the on-time of the switch Sw, the current in the inductor rises; during the off-time of the switch Sw, the current in the inductor decreases. If the current in the inductor drops to zero during the off-time of the switch Sw, and the energy kept in the inductor is also zero during the remaining off-time, then the switching power supply is said to operate in the discontinuous conduction mode (DCM); otherwise, it operates in the continuous conduction mode (CCM) [18], [19]. The following analyzes the two operating modes of the boost DC-DC switching converter to facilitate system design.

2.2. Continuous Conduction Mode (CCM)

The Heading uses ton to represent the on-time of the switch tube and toff to represent the off-time of the switch tube. Ts represents a switching cycle. During operation, when the gate control pulse turns on the switch tube Sw, the capacitor C starts to charge, and the output voltage Vo applied to the load resistor R_L rises. During the charging process of capacitor C, the current in the inductor L gradually rises, and the stored magnetic field energy also gradually increases. After the on-time ton, the gate control pulse turns off the switch tube Sw, the current in the inductor L decreases, and the induced potential generated at both ends of L turns on the freewheeling diode V_D, and the magnetic field energy kept in L is transported to the load through V_D. When the output voltage Vo is inferior to the voltage across the capacitor C, the capacitor C discharges to the load. When the next cycle arrives, the gate control pulse turns on the switch again, and the above process repeats [20], [21]. The waveforms of each point in the circuit are shown in Fig. 2.

When the gate control pulse turns on the switch, the current in the inductor L rises from the minimum value $i_{L,min}$ to the maximum value $i_{L,max}$. When the gate control pulse turns off the switch, the current in L reduces from the maximum value $i_{L,max}$ to the minimum value $i_{L,min}$. During the time of the switch, the inductor voltage can be articulated as

$$V_L = V_i = L\frac{di_L}{dt} \tag{1}$$

From this can get

$$\Delta I_{L(+)} = \frac{1}{L}\int V_i dt = \frac{V_i}{L}t_{on} \tag{2}$$

When the switch conduction state ends (t=ton), the current in the inductor L spreads to the maximum value iL, max.

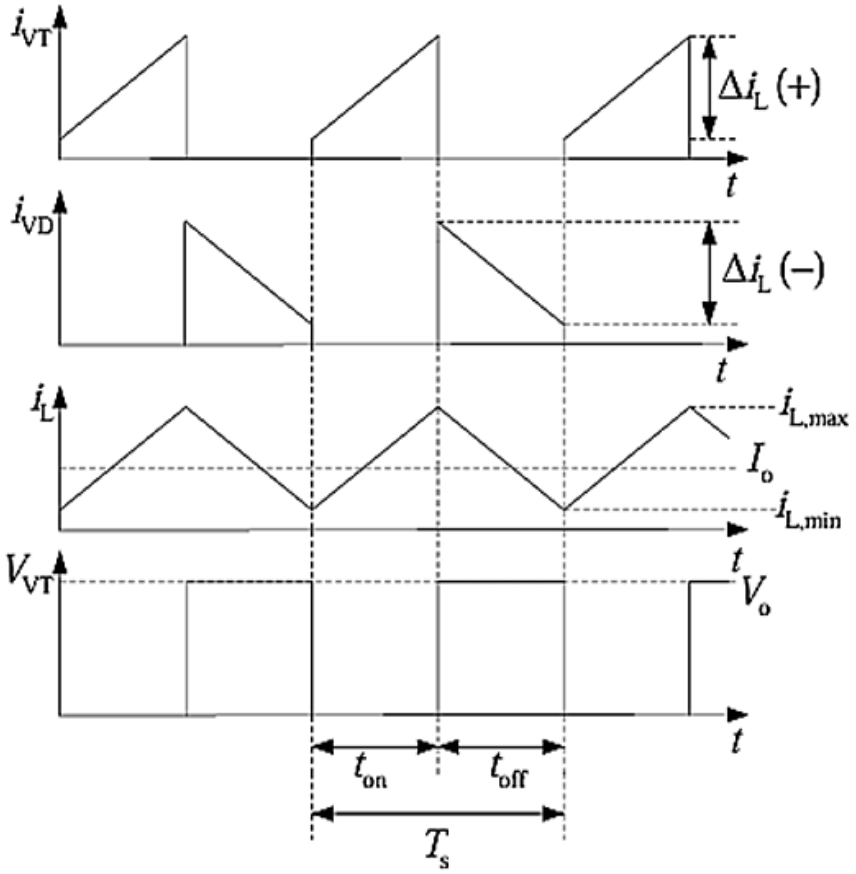

Fig. 2. CCM working mode waveform

$$i_{L,max} = \frac{V_i}{L} t_{on} + i_{L,min} \tag{3}$$

When the switch is turned off, the current in the inductor L releases energy to the burden through the freewheeling diode VD and can get

$$V_o - V_i = -L \frac{di_L}{dt} \tag{4}$$

$$\Delta I_{L(-)} = -\frac{1}{L} \int (V_o - V_i) dt = \frac{-V_o + V_i}{L} t_{off} \tag{5}$$

When the switch cut-off state ends (t=toff), the current in the inductor L drops to the minimum value IL, min.

$$i_{L,min} = \frac{-V_o + V_i}{L} t_{off} + i_{L,max} \tag{6}$$

According to the volt-second balance principle, it can be attained from equations (2) and (5).

$$V_o = \frac{1}{1 - D} V_i \tag{7}$$

Where D = ton/Ts is the duty cycle of the switch tube. Equation (7) is the output and input voltage relationship when the Boost DC-DC converter works in CCM. The output voltage Vo rises monotonically with the rise of the duty cycle D of the switch tube. Since the duty cycle D is always less than 1, Vo is always greater than Vin, so the Boost converter is often called a boost switching converter [22].

2.3. Discontinuous Conduction Mode (DCM)

Assuming that DTs represent the time when the switch is turned on, D_1Ts represent the time when the switch is turned off until the inductor current continues to reduce until it reaches zero, and D_2Ts represent the time when the inductor current remains zero, then D = 1- D_1- D_2. The working principle of the discontinuous conduction mode is analyzed as follows: During the operation, the gate control pulse turns on the switch Sw, the capacitor C starts to charge, the output voltage Vo rises, and the current in the inductor L gradually increases from zero. The freewheeling diode V_D is now cut off due to reverse bias. After the on-time DTs, the switch is cut off, the current in L decreases, the induced potential generated at both ends of L turns on VD, and the magnetic field energy kept in L is transported to the load through the freewheeling diode V_D. When the load voltage is lower than at both ends of capacitor C, capacitor C begins discharging to the load [23], [24]. After the off-time D_1Ts, the current in the inductor reduces to zero, and the output voltage is maintained entirely by the discharge of capacitor C to the load. After D_2Ts, the control pulse signal turns on the switch again, and the above process repeats. The waveforms of each node of the circuit are illustrated in Fig. 3.

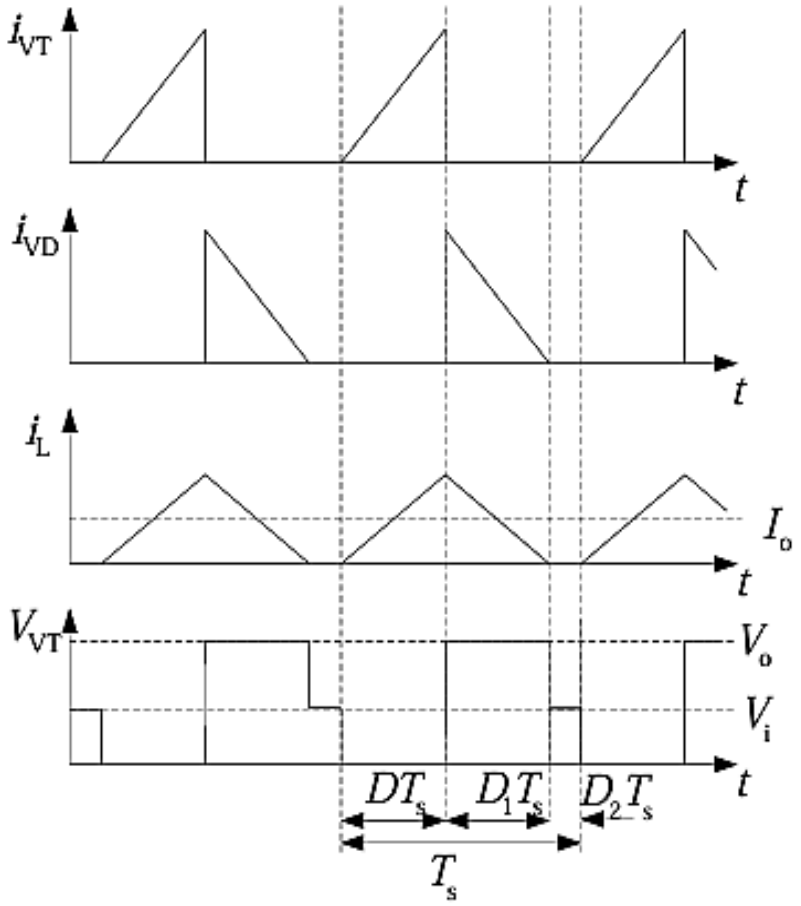

Fig. 3. DCM working mode waveform

According to the volt-second balance principle, it has

$$V_i DT_s = (V_o - V_i)D_1T_s \tag{8}$$

From formula (8), it can be obtained.

$$\frac{V_o}{V_i} = \frac{D + D_1}{D_1} \tag{9}$$

Assume no loss in power conversion, Pi = Po is

$$\frac{I_i}{I_o} = \frac{D + D_1}{D_1} \tag{10}$$

Assume no loss in power conversion, Pi = Po is

$$\Delta I_L = \frac{V_o - V_i}{L} D_1 T_s \tag{11}$$

Substituting equation (8) into equation (11), it gets

$$\Delta I_L = \frac{V_i}{L} D T_s \tag{12}$$

Then, the input current can be expressed as

$$I_i = I_L = \frac{1}{2} \Delta I_L (D + D_1) \tag{13}$$

From formula (10), it can be obtained.

$$I_i = \frac{D + D_1}{D_1} I_o = \frac{D + D_1}{D_1} \frac{V_o}{R_L} \tag{14}$$

Combining equations (13) and (14) and substituting equation (9) into equation can be obtained.

$$D_1^2 - \frac{2L}{D R_L T_s} D_1 - \frac{2L}{R_L T_s} = 0 \tag{15}$$

Thus, it can get.

$$D_1 = \frac{2L}{D R_L T_s} \left[1 + \sqrt{(1 + \frac{2D^2 R_L T_s}{L})} \right] \tag{16}$$

Substituting equation (16) into equation (9) yields.

$$\frac{V_o}{V_i} = \frac{1 + \sqrt{(1 + \frac{2D^2 R_L T_s}{L})}}{2} \tag{17}$$

Equation (17) is the output and input voltage relationship when the Boost DC-DC switching converter operates in DCM.

3. PI Control Scheme for Boost Circuit

Since most current control methods for boost circuits use traditional PI control, they have the advantages of a simple structure and high reliability. Still, the system's dynamic characteristics and anti-interference performance need further improvement [25]. Since the predictive PI control algorithm can resist hysteresis and suppress negative regulation, it is applied to the boost circuit for theoretical research and real-time simulation. The main research topic of this chapter is to compare the dynamic response characteristics of the boost circuit under the predictive PI mechanism algorithm and the traditional PI control [26]. Since the boost circuit is a typical DC-DC power converter, and the transfer function of the controlled object has a non-minimum phase characteristic, it is manifested as a zero point in the right half plane in the small signal mathematical model. A significant feature of these zero points is that, in the event of an unexpected alteration in the duty cycle, the output voltage will first drop and then rise at the beginning of the cycle; negative regulation will occur [27]. This negative regulation phenomenon will degrade the control system's dynamic performance and prolong the system's transition time. Therefore, it is very important to suppress negative regulation for the boost circuit. Because of the nonlinear characteristics of the aforementioned boost circuit, this chapter

uses a predictive PI control algorithm to control it [28], [29]. The simulation results show that the predictive PI mechanism algorithm provides good control [30]. The model PI control block diagram of the boost converter is displayed in Fig. 4.

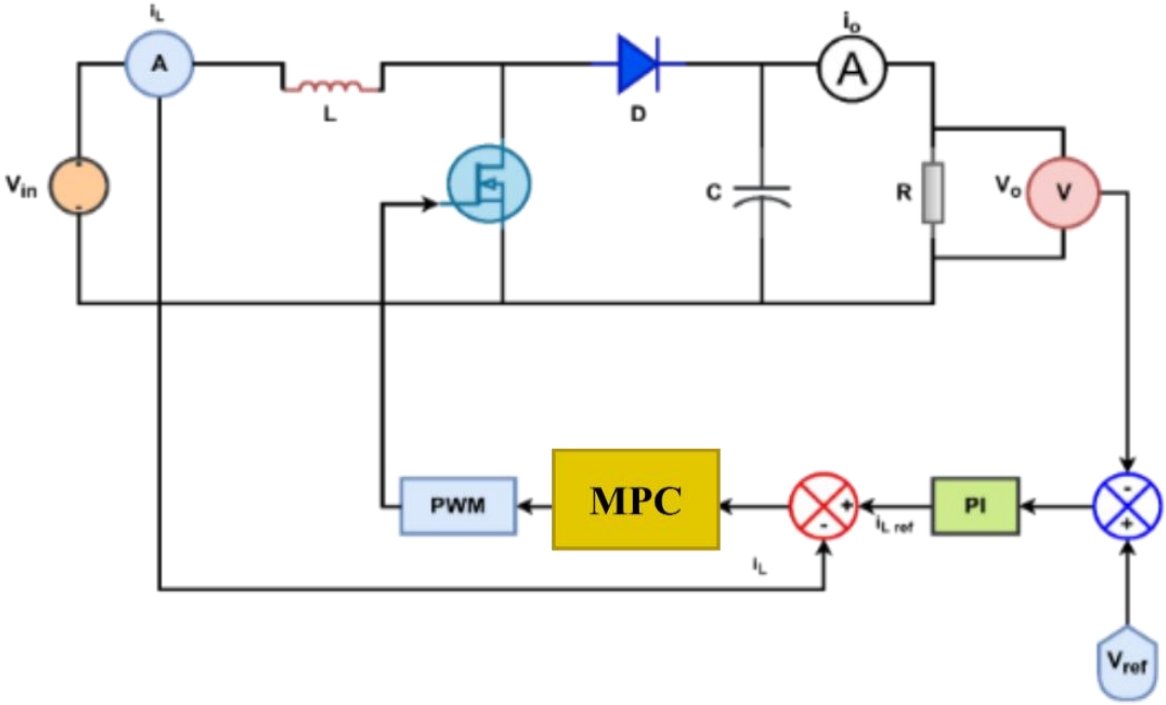

Fig. 4. The block illustration of PI-MPC

3.1. Model Predictive Control

MPC is based on the following principle: a finite number of switching states can be shaped by a static power converter, and the system model is used to predict the change characteristics of the variables associated with each switching state. The objective function is defined and minimized to evaluate the expected value of the control variable for each switching state, and the switching state that minimizes the objective function is designated as the next switching state [31], [32]. The switch state of the switch tube at the moment. The model-prediction control block for the boost converter is illustrated in Fig. 4. It comprises two steps: establishing the prediction model and optimizing performance. Among them, the prediction model is established based on an equivalent circuit for all the converter's switching states, and performance optimization comprises two steps: defining the objective function and selecting the switching state that minimizes it [33], [34].

The voltage outer loop is utilized to produce the orientation current of the converter, and the MPC is utilized to track the orientation current [35]. The specific control flow is shown in Fig. 5.

The model prediction is established by taking the bidirectional DC-DC converter working in Boost mode as an example. The converter model and its possible switching states are analyzed in detail [36]. Two switching states for the bidirectional DC-DC converter are working in Boost mode. The equivalent circuit of the converter in each switching state is displayed in Fig. 1. Kirchhoff's law can obtain the discretized equation corresponding to each set of switching states in the equivalent circuit [37]. Then, the prediction model under different switching states can be obtained. As shown in Fig. 1, the Boost converter topology is displayed in Fig. 1, where: S is a controllable switch tube; D is a diode; L and RL are the inductance and resistance of the inductor; C and RC are the output capacitor and its parasitic resistance; Vo is the output voltage; Vin is the input voltage.

The Boost converter's one-step predictive output voltage control must first control the inductor current [38], [39]. Since this paper mainly focuses on the MPC control algorithm, a continuous-time

model must be established. The general model predictive control principle of a DC/DC converter is displayed in Fig. 6.

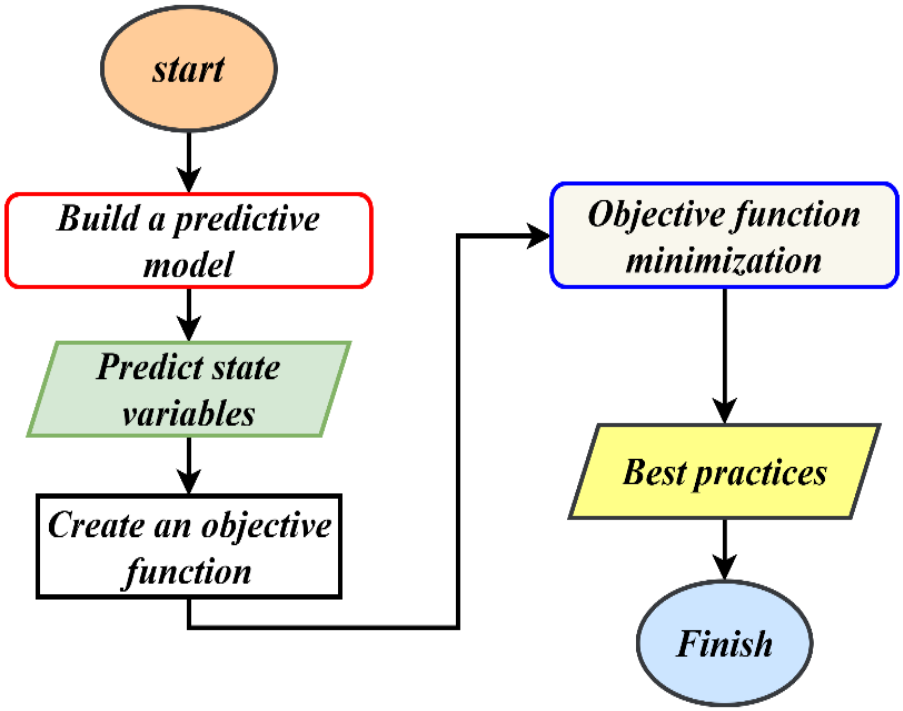

Fig. 5. Model predictive control flow chart

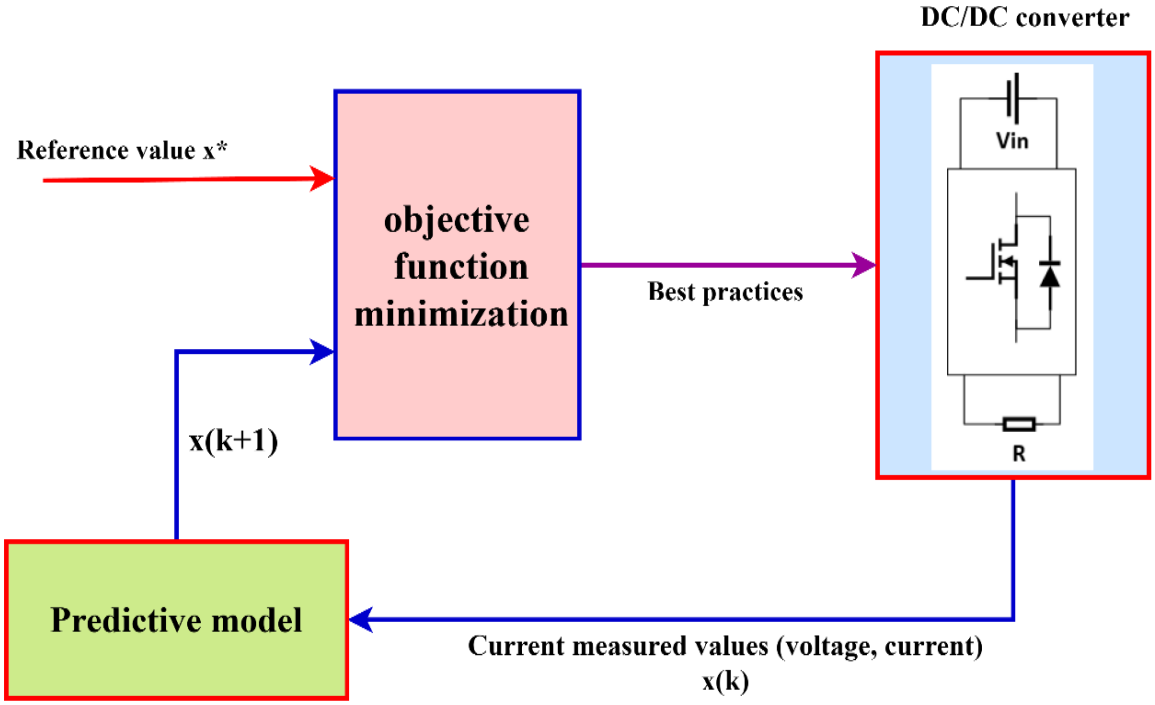

Fig. 6. General model predictive control schematic

Among them, the continuous time model is:

$$\frac{di_{L(t)}}{dt} = \frac{V_{in} - R_L i_{L(t)}}{L} + (u_{(t)} - 1)\frac{V_{o(t)}}{L} \quad (18)$$

$$\frac{dV_{o(t)}}{dt} = \frac{1-u_{(t)}}{C} i_{L(t)} - \frac{V_{o(t)}}{RC} \tag{19}$$

$$u_{(t)} = \begin{cases} 1, S = 1 \\ 0, S = 0 \end{cases} \tag{20}$$

Where: u(t) is the input of the system, indicating the switch state of the switch tube; S=1 means the switch is closed, and S=0 means the switch is open. The discrete-time model is:

$$i_{L(k+1)} = \left(1 + \frac{R_L T_s}{L}\right) i_{L(k)} + \left(u_{(k)} - 1\right) \frac{V_{o(k)} T_s}{L} + \frac{V_{in} T_s}{L} \tag{21}$$

$$V_{o(k+1)} = \frac{T_s}{L} i_{L(k)} + \left(1 - \frac{T_s}{RC}\right) V_{o(k)} - \frac{T_s}{L} u_{(k)} i_{L(k)} \tag{22}$$

Performance optimization, as described in 23, is the application scenario that puts forward the following performance requirements for the converter [40], [41]. Let the actual current follow the reference current value change. Define the cost function as

$$J_k = [i_{Lref} - i_{L(k+1)}]^2 \tag{23}$$

4. Linear Active Disturbance Rejection Controller (LADRC)-MPC

MPC optimization: The LADRC controller is used as the boost converter. Considering that in the actual system, if the input voltage fluctuation or load mutation occurs in the Boost converter system, it will affect the unchanging output of the system. Combined with the above, a mechanism scheme created on LADRC is suggested. First, the LADRC controller is constructed with the output voltage and the inductor current Li as the state variables, and the cascade method is used to address the drawbacks of narrow bandwidth and poor dynamic performance caused by the non-minimum phase characteristics of the converter. The specific implementation method estimates the system state and disturbance by establishing ESO so that the system becomes a linear integral system. Then, a simple PD controller compensates for the control requirements.

The structure diagram is demonstrated in Fig. 7. The model prediction control block illustration of the boost converter is displayed in Fig. 8.

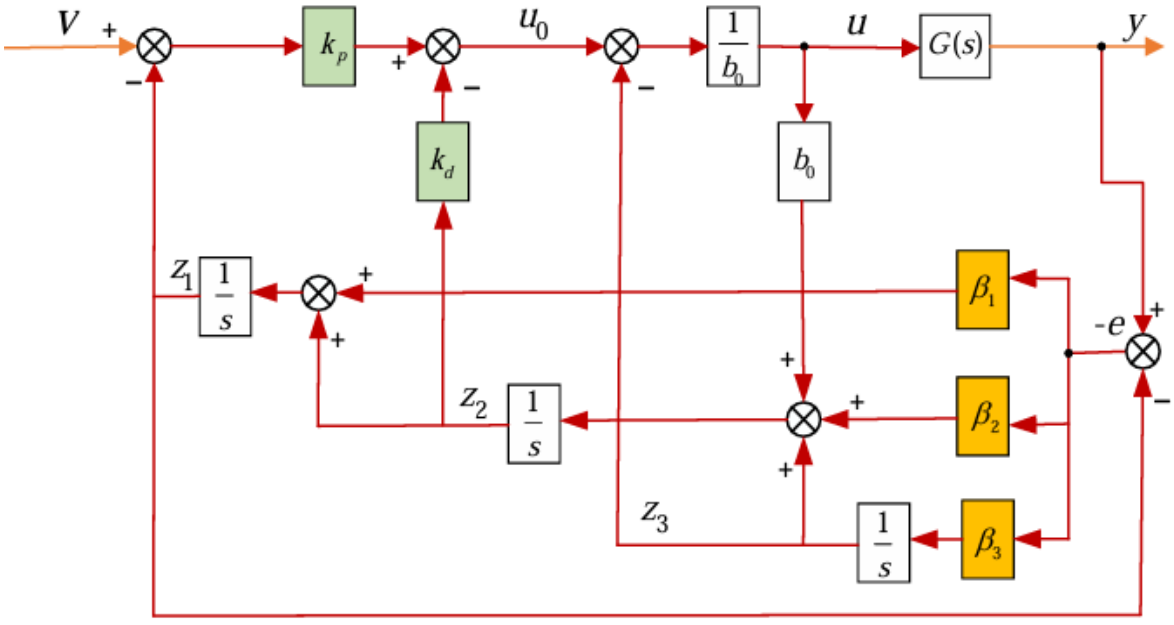

Fig. 7. LADRC control of the boost converter

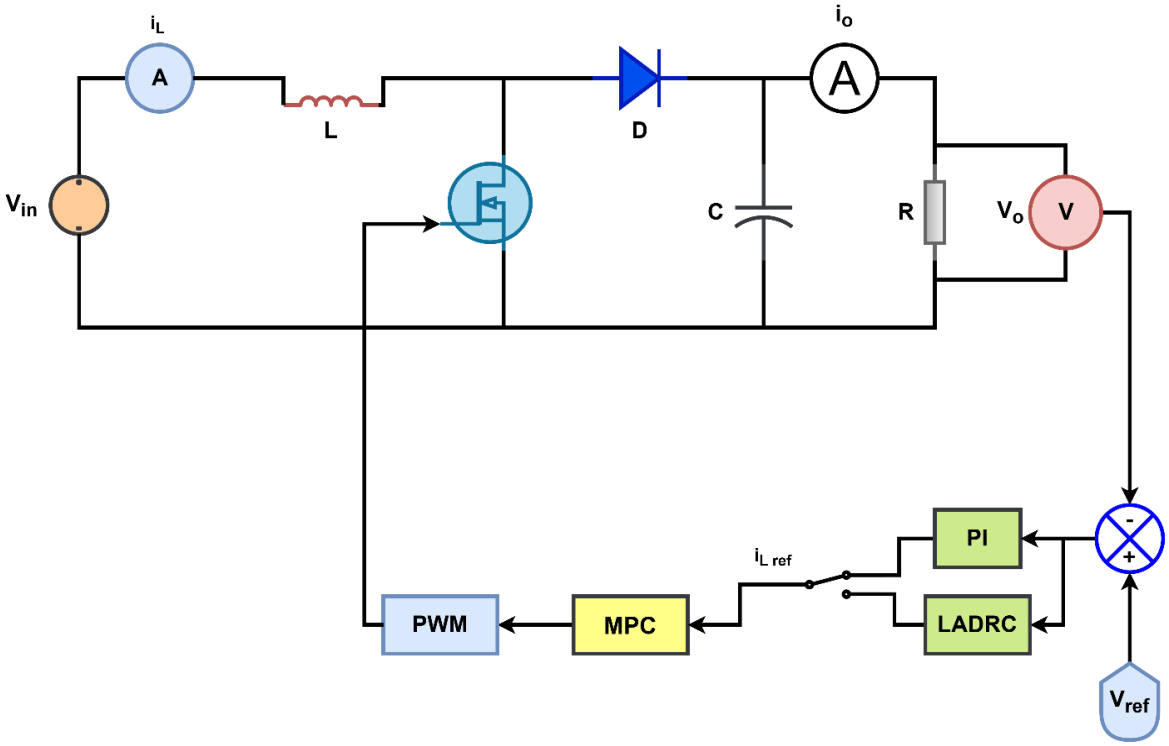

Fig. 8. Block illustration of LADRC-MPC

First, the following LESO equation is established withV_o As the state variable:

$$\dot{Z}_1 = Z_2 - \beta_1(Z_1 - V_o) \tag{24}$$

$$\dot{Z}_1 = Z_2 - \beta_1(Z_1 - V_o) \tag{25}$$

$$\dot{Z}_2 = Z_3 - \beta_2(Z_1 - V_o) + b_o i_{Lref} \tag{26}$$

$$\dot{Z}_3 = \beta_3(Z_1 - V_o) \tag{27}$$

Where $Z_1 = \hat{V}_o$; is the V_o estimated value, Z_1 is the $\hat{V}_o$ of the derivative, Z_3 is an estimate of the total disturbance, i_{Lref} Is the reference value of i_L, $\beta_1, \beta_2, \beta_3 > 0$ is the observer parameter, b_o Is the estimated value of the controller gain b? By choosing the appropriate, $\beta_1, \beta_2, \beta_3$LESO can complete the real-time tracking of each variable. The waveform is illustrated of Z_3 Shown in Fig. 9. Let the control law be:

$$i_{Lref} = \frac{-Z_3 + u_o}{b_o} \tag{28}$$

Ignoring the estimation error of Z_3 For the total disturbance, the controlled system can be transformed into a double-integral series structure, where 0u selects the PD controller as:

$$u_o = k_p(V_{ref} - Z_1) - k_d Z_2 \tag{30}$$

In the formula, V_{ref} Is the given voltage reference value k_p, k_d Are the parameters of the PD controller? The closed-loop transfer function of the system can be obtained from the previous formula:

$$G_{cl} = \frac{k_p}{S^2 + k_d S + k_p} \tag{31}$$

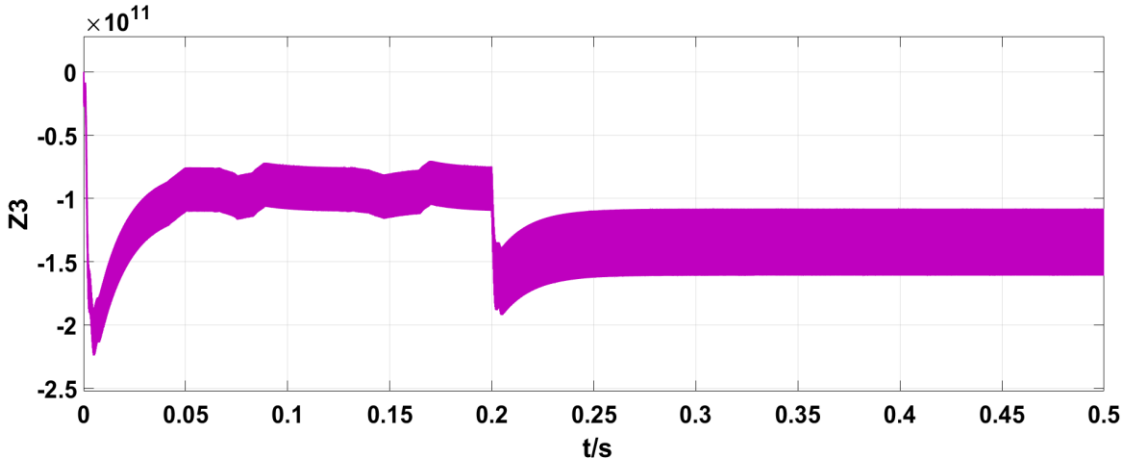

Fig. 9. The waveform is illustrated of Z_3

By selecting appropriate k_p, k_d The system can be stabilized. The property equation of LESO can be further attained as:

$$S^3 + \beta_1 S^2 + \beta_2 S + \beta_3 = (S + w_{cl})^3 \tag{32}$$

Then there is $\beta_1 = 3w_{cl}, \beta_2 = 3w_{cl}^2, \beta_3 = w_{cl}^3$

Similarly, the control bandwidth of the controller is configured to be w_{cl}, so that:

$$S^2 + k_d S + k_p = (S + w_{cl})^2 \tag{33}$$

Then there is $k_d = 2w_{cl}, k_p = w_{cl}^2$

5. Results and Discussion

To utterly determine and validate the functional efficiency of the Boost preacher when executed under the control methodology famous as Linear Active Disturbance Rejection Control (LADRC), a carefully built imitation model was developed applying the leading competencies of MATLAB/Simulink spreadsheet. Furthermore, this simulation promoted an inclusive approximate analysis that wanted to place side by side the act consequences of the LADRC control method against those obtained for a normal PI control order, particularly meeting on synopsizes from differences in the reference power.

The principal revolution limits suitable for the Boost converter that have been particularly devised for this review are orderly written in Table 1, while the parameters guide the LADRC boss are carefully particularized in Table 2; furthermore, the limits relevant to the PI boss are also bestowed in Table 2 for further clarity and approximate analysis.

Table 1. Shows the parameters of the boost converter

Parameter	Value	Parameter	Value
DC bus voltage	30V	Resistance load	10Ω
Capacitance	100μF	Inductance	1mH

Table 2. Shows the parameters of the LADRC controller and PI

Parameter	Value
Observer bandwidth	1000000
Controller bandwidth w_{cl}	4000
Controller gain	10000000000
Kp	0.03
Kd	2

5.1. Case 1 Changes the Voltage From 50 to 60 V

When the citation potential is modified from 50 V to 60 V, while different limits remain constant, the fake crop-generated power waveform is illustrated in Fig. 10 and Fig. 11. As proved for one figure, the gain startup time of bureaucracy promoting the LADRC-MPC control methods demonstrates an obvious improvement distinguished from the earlier two methods, presenting diminished overshoot. In instances of unexpected changes in the remark heat, the improvement time of the harvest's physical ability to a stable state is notably shorter than that noticed accompanying the prior two methods. At ts=0.2, the citation generated power transitions from 50V to 60V.

The figure displays that the adaptation time of the Boost preacher engaging the LADRC-MPC control approach is 22ms, whereas the adaptation time for the PI-MPC is 80ms. The union occasion when the citation power is changed is written at 22ms, which is considerably superior to that of the different control structures.

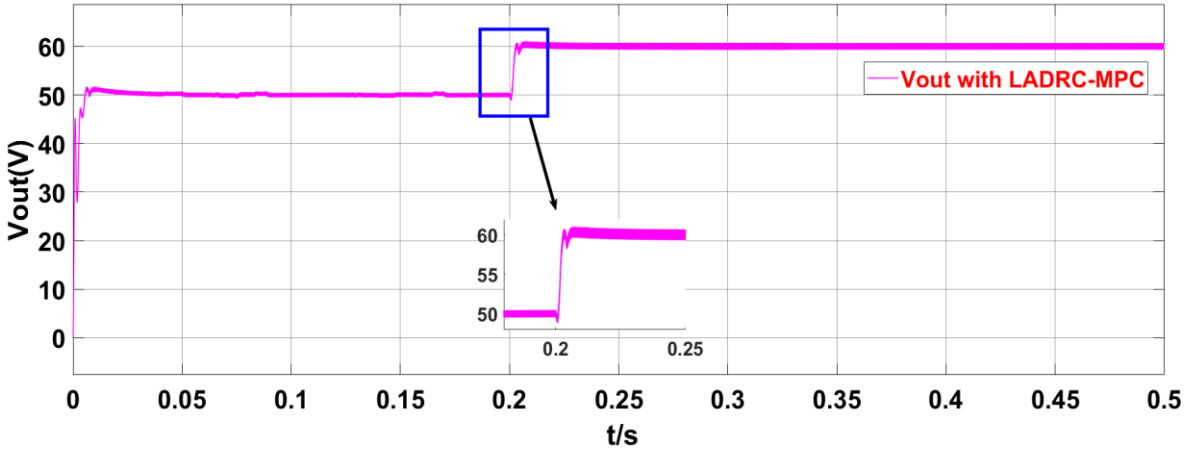

Fig. 10. Output voltage waveforms with LADRC-MPC

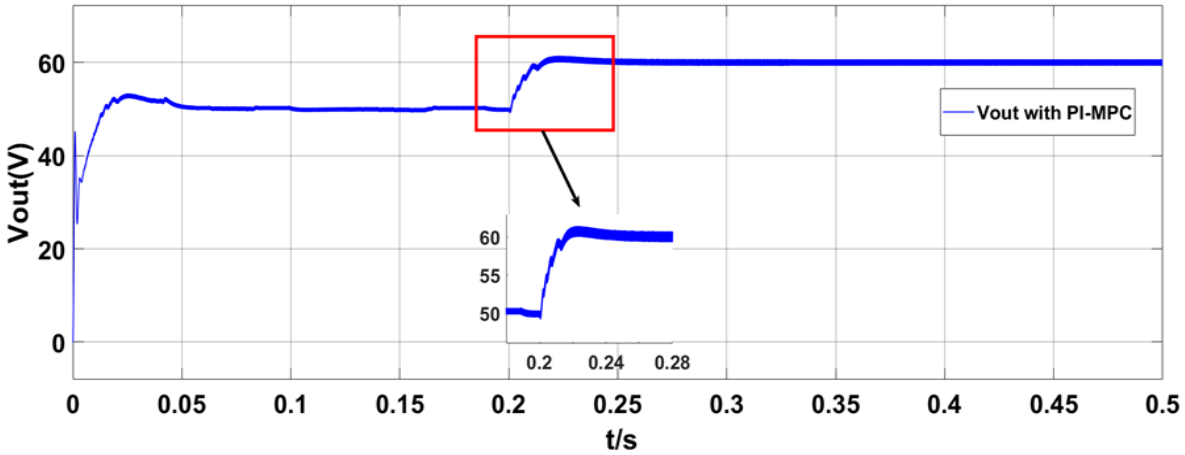

Fig. 11. Output voltage waveforms with PI-MPC

Fig. 12 and Fig. 13 support an inclusive illustration of the profit current waveform, which serves as a fault-finding component in understanding the conduct characteristics of the Boost preacher under miscellaneous control arrangements. It is important that the reference strength knowledge shows a meaningful increase from 50V to 60V exactly at the moment designated as ts=0.2, displaying a particular stage where detracting changes happen inside the system. The dossier bestowed in the figure obviously signifies that the adjustment occasion necessary for the Boost preacher appropriating the LADRC-MPC control methodology is a unusually adept 12ms, when in fact the adaptation time longer to 27ms when engaging the PI-MPC control action. In an approximate analysis of these two different

control plans, it is apparent that the convergence opportunity noticed when the remark capacity experiences an alternative is an absolute 12ms accompanying the LADRC-MPC design, which starkly achieves superior performance compared to the other two control actions, that is to say PI-MPC. This note not only emphasizes the adeptness of the LADRC-MPC approach but likewise plans a irresistible advantage in control exercise for requests needing rapidly generated power adaptations. Therefore, the dossier elucidated in this place figure serves as a valuable reference for scientists and engineers aiming to improve the functional efficacy of Boost converters in vital atmospheres.

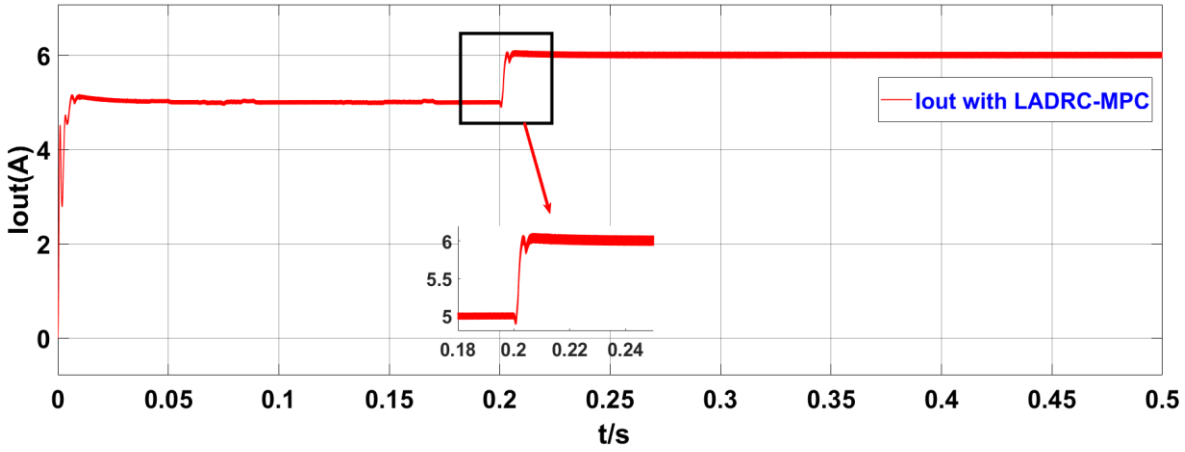

Fig. 12. Output current waveforms with LADRC-MPC

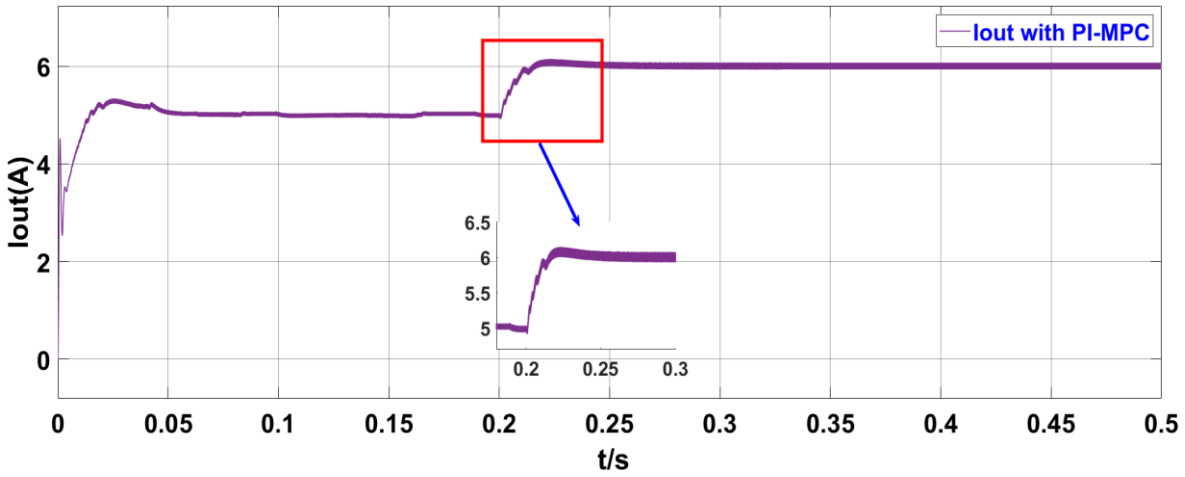

Fig. 13. Output current waveforms with PI-MPC

5.2. Case 2 Changes the Voltage From 60 to 50 V

Fig. 14 and Fig. 15 depict the waveform of the yield strength. The request of the LADRC-MPC control methodology remarkably improves the bureaucracy's manufacturing startup event, and the improvement breaks down to a stable state when the reference strength changes from 60V to 50V. The adaptation event for the Boost preacher is characterized at 20ms for LADRC-MPC, opposite to 26ms for the PI-MPC order. The convergence event is further significantly superior. The power output ranges from 60.06V to 59.95V in the LADRC-MPC arrangement. Consequently, distinguished from the Boost preacher system controlled by PI-MPC, the heat output is written at 60.062V to 59.82V. The LADRC-MPC framework demonstrates a reduced overshoot and an accelerated convergence rate.

Fig. 16 and Fig. 17 depict the waveform associated with the output current. The implementation of the LADRC-MPC control methodology significantly improves both the output startup duration of the system and the recovery time to a steady state when the reference voltage transitions from 60V to 50V. The adjustment period for the Boost converter is measured at 80ms for the LADRC-MPC

approach, in contrast to 50ms for the PI-MPC framework. The convergence time is also markedly more favorable. The LADRC-MPC architecture exhibits a diminished overshoot and an enhanced rate of convergence.

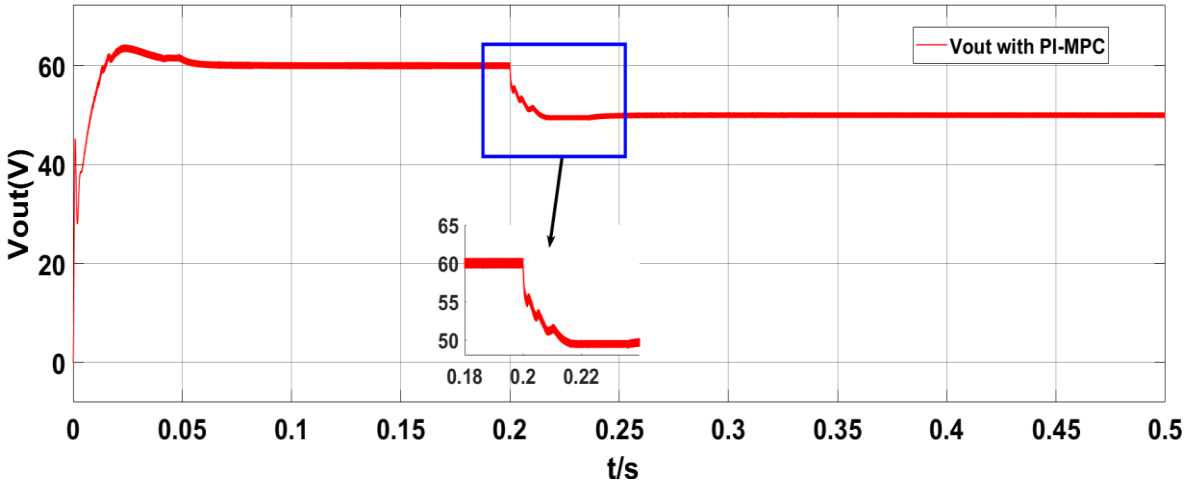

Fig. 14. Output voltage waveforms with LADRC-MPC

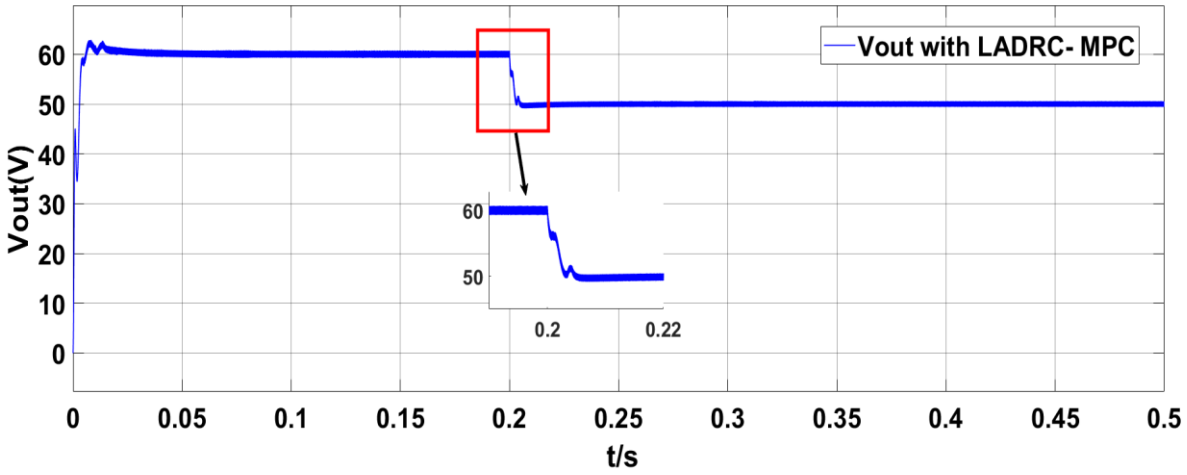

Fig. 15. Output voltage waveforms with PI-MPC

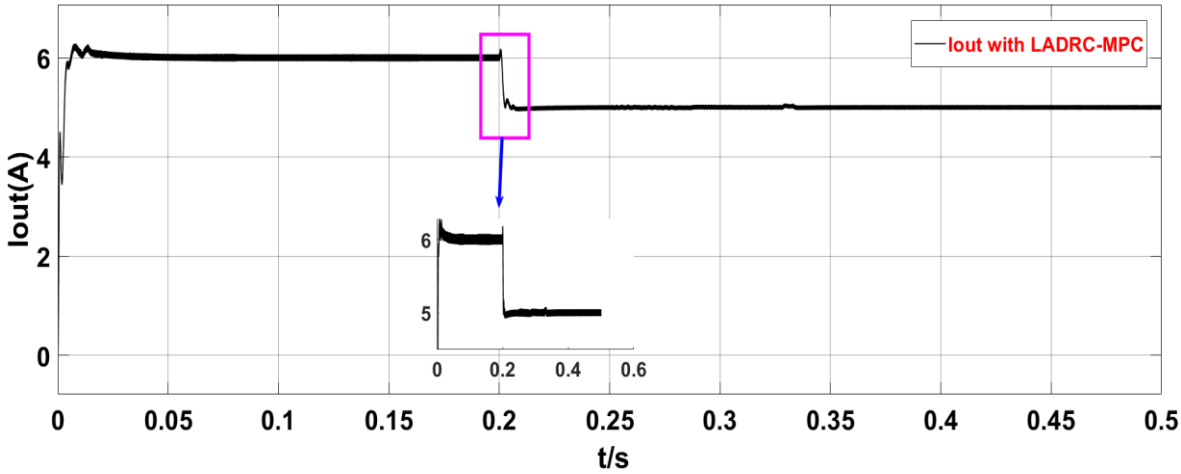

Fig. 16. Output current waveforms with LADRC-MPC

5.3. Case 3 Change in Load Resistance

Fig. 18 and Fig. 19 depict the waveform associated with the output current. The reference voltage maintains a steady state of 60V during the alteration of load resistance at ts=0.2. Fig. 18 and Fig. 19 demonstrate that the adjustment duration of the Boost converter is 4ms when employing the LADRC-MPC control methodology, while it is 30ms when implementing the PI-MPC approach. In contrast to the previously mentioned control systems, the convergence time in response to fluctuations in the reference voltage is recorded at 4ms, signifying a noteworthy enhancement.

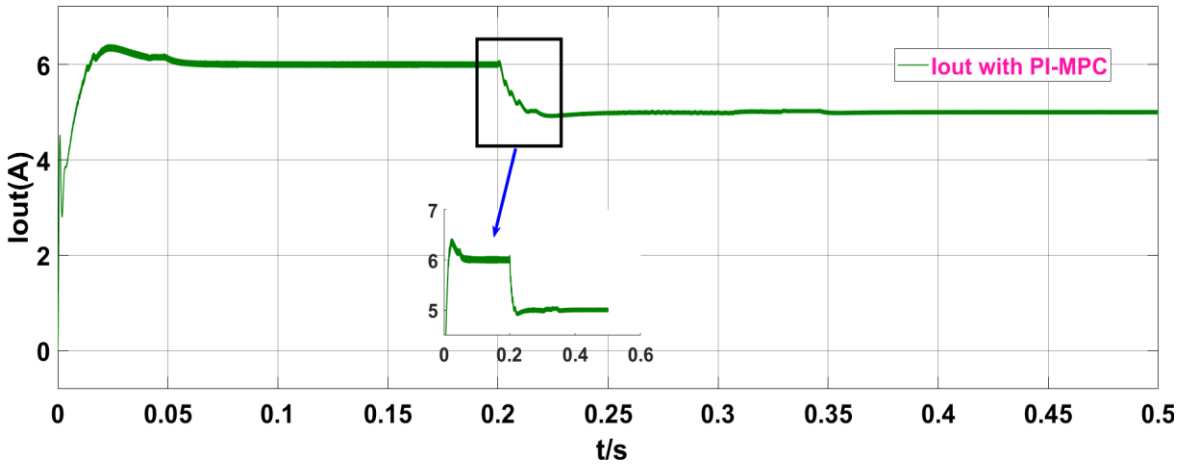

Fig. 17. Output current waveforms with PI-MPC

Within the LADRC-MPC paradigm, the identified overshoot is quantified as 7.251A to 7.118A. As a result, the voltage overshoot is noted to be 7.302A to 7.195A within the Boost converter governed by the PI-MPC control strategy.

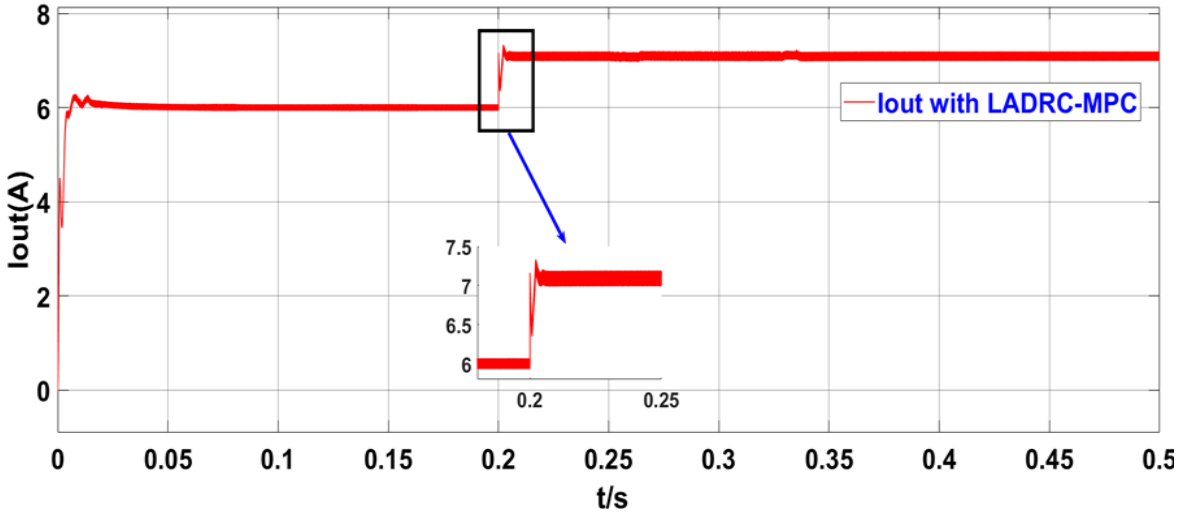

Fig. 18. Output current waveforms with LADRC-MPC

Through an extensive and meticulous examination of the extensive dataset that has been meticulously gathered from the series of experiments that were methodically carried out, it becomes increasingly apparent that the information summarized within Table 3 serves to vividly and comprehensively illustrate a thorough and detailed comparison among the three distinctly different methodologies that have been systematically implemented throughout the course of this research, and the findings derived from this analysis unequivocally indicate that the method proposed in this study consistently yields outcomes that are not only markedly superior in terms of quality but also exhibit a significant degree of effectiveness when placed in direct juxtaposition with the performance metrics

associated with the two control systems that were utilized as benchmarks within the context of this comprehensive investigation.

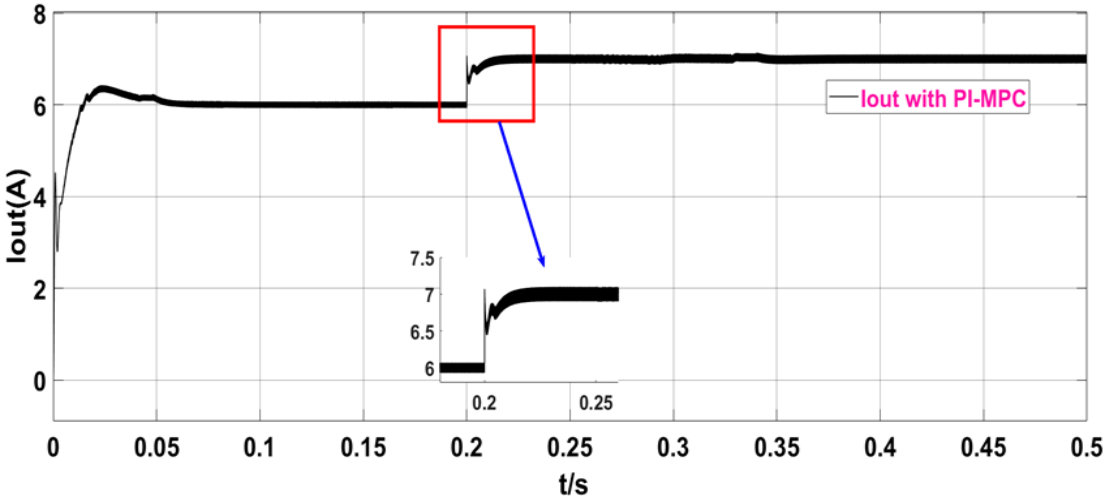

Fig. 19. Output current waveforms with PI-MPC

Table 3. Shows the comparison between the three methods

Method	Adjustment Time of the Current	Adjustment Time of the Voltage
	Case 1	
PI-MPC	0.027 s	0.08s
LADRC-MPC	0.012 s	0.022s
	Case 2	
	The overshoot of the current	The overshoot of voltage
PI-MPC	6.015A~5.93A	60.5V~59.82V
LADRC-MPC	6.006A~5.998A	60.06V~59.95V
	Case 3	
	adjustment time of the current	The overshoot of the current
PI-MPC	0.03s	7.302A~7.195A
LADRC-MPC	0.004s	7.251A~7.118A

6. Conclusion

In this academic item, the basic circuitry of the BOOST preacher is originally distinguished, including two constant-state and dynamic reactions. Building upon this support, the strength of the BOOST preacher method employing the voltage control loop is precisely checked. Ultimately, with the understanding of the bureaucratic rules of the BOOST preacher, the improved methods are developed and implemented through MATLAB. A growth (LADRC) algorithm is projected to establish predicting strength central loop control. The treasure solved the questions of slow active reaction and waveform deformity of loop PI control. The consequences of the imitation indicate that the projected methods exhibit praiseworthy balance. Using the MATLAB floor, the functional implementations of the established PI-MPC control invention and the LADRC-MPC control treasure were distinguished. Through unending discipline and calibration processes, imitation results were got, ratifying that the process control effect utilizing the LADRC-MPC invention is superior.

This reinforces the establishment, speed, and efficiency concerning this treasure in agreements of control effect, professed its influence. Through an inclusive reasoning of the moment of truth domain of the unoriginal PI and PI-MPC, alongside the vital act of the developed LADRC-MPC boss, it is ascertained that the LADRC-MPC order displays reduced omission and sped up union speed. In the context of LADRC-MPC, the overshoot is currently recorded at 6.006A~5.998A. Consequently, the voltage overshoot is observed to be 7.302A~7.195A within the PI-MPC-controlled Boost converter system and 7.251A~7.118A in the PI-MPC-controlled configuration. Future work will involve adding constraints to the objective function.

Author Contribution: All authors contributed equally to the main contributor to this paper. All authors read and approved the final paper.

Funding: This research received no external funding.

Conflicts of Interest: The authors declare no conflict of interest.

References

[1] R. S. Inomoto, J. R. B. d. A. Monteiro and A. J. S. Filho, "Boost Converter Control of PV System Using Sliding Mode Control With Integrative Sliding Surface," *IEEE Journal of Emerging and Selected Topics in Power Electronics*, vol. 10, no. 5, pp. 5522-5530, 2022, https://doi.org/10.1109/JESTPE.2022.3158247.

[2] N. A. Ahmed, B. N. Alajmi, I. Abdelsalam and M. I. Marei, "Soft Switching Multiphase Interleaved Boost Converter With High Voltage Gain for EV Applications," *IEEE Access*, vol. 10, pp. 27698-27716, 2022, https://doi.org/10.1109/ACCESS.2022.3157050.

[3] K. A. Singh, A. Prajapati and K. Chaudhary, "High-Gain Compact Interleaved Boost Converter With Reduced Voltage Stress for PV Application," *IEEE Journal of Emerging and Selected Topics in Power Electronics*, vol. 10, no. 4, pp. 4763-4770, 2022, https://doi.org/10.1109/JESTPE.2021.3120802.

[4] M. K. Ismae, S. T. Bahar, and A. A. Abdullah, "Harmonic Elimination Method for Permanent Magnet Synchronous Motor Utilizing Active Disturbance Rejection Control," *Proceedings of Engineering and Technology Innovation*, vol. 30, pp. 11-23, 2025, https://doi.org/10.46604/peti.2024.14386.

[5] T. Arunkumari and V. Indragandhi, "A review on single switch Dc-Dc converter for renewable energy based applications," *2017 Innovations in Power and Advanced Computing Technologies (i-PACT)*, pp. 1-5, 2017, https://doi.org/10.1109/IPACT.2017.8245114.

[6] M. Veerachary and P. Kumar, "Analysis and Design of Quasi-Z-Source Equivalent DC–DC Boost Converters," *IEEE Transactions on Industry Applications*, vol. 56, no. 6, pp. 6642-6656, 2020, https://doi.org/10.1109/TIA.2020.3021372.

[7] S. Pirpoor, S. Rahimpour, M. Andi, N. Kanagaraj, S. Pirouzi and A. H. Mohammed, "A Novel and High-Gain Switched-Capacitor and Switched-Inductor-Based DC/DC Boost Converter With Low Input Current Ripple and Mitigated Voltage Stresses," *IEEE Access*, vol. 10, pp. 32782-32802, 2022, https://doi.org/10.1109/ACCESS.2022.3161576.

[8] P. Mohseni, S. Mohammadsalehian, M. R. Islam, K. M. Muttaqi, D. Sutanto and P. Alavi, "Ultrahigh Voltage Gain DC–DC Boost Converter With ZVS Switching Realization and Coupled Inductor Extendable Voltage Multiplier Cell Techniques," *IEEE Transactions on Industrial Electronics*, vol. 69, no. 1, pp. 323-335, 2022, https://doi.org/10.1109/TIE.2021.3050385.

[9] G. Li, X. Jin, X. Chen, and X. Mu, "A novel quadratic boost converter with low inductor currents," *CPSS Transactions on Power Electronics and Applications*, vol. 5, no. 1, pp. 1-10, 2020, https://doi.org/10.24295/CPSSTPEA.2020.00001.

[10] S. T. Bahar and Y. G. Rashid, "A Study on an MPPT Control Approach Using Artificial Intelligence and the Perturb and Observe Method," *Diyala Journal of Engineering Sciences*, vol. 17, no. 2, pp. 131-143, 2024, https://doi.org/10.24237/djes.2024.17210.

[11] M. Dasohari, N. Vishwanathan, S. Porpandiselvi and A. R. M. Vani, "A Soft-Switched Boost Converter Based LED Driver With Reduced Input Current Ripple," *IEEE Access*, vol. 12, pp. 45904-45922, 2024, https://doi.org/10.1109/ACCESS.2024.3377122.

[12] M. Veerachary and M. R. Khuntia, "Design and Analysis of Two-Switch-Based Enhanced Gain Buck–Boost Converters," *IEEE Transactions on Industrial Electronics*, vol. 69, no. 4, pp. 3577-3587, 2022, https://doi.org/10.1109/TIE.2021.3071696.

[13] C. -Y. Chan, S. Chincholkar and W. Jiang, "A Modified Fixed Current-Mode Controller for Improved Performance in Quadratic Boost Converters," *IEEE Transactions on Circuits and Systems II: Express Briefs*, vol. 67, no. 10, pp. 2014-2018, 2020, https://doi.org/10.1109/TCSII.2019.2942057.

[14] L. K. Dangeti, G. Chilakalapudi and A. Kumar, "An improved Hybrid switched inductor and switched capacitor based DC-DC Converter to reduce the voltage stress across the switch," *2023 IEEE Silchar Subsection Conference (SILCON)*, pp. 1-5, 2023, https://doi.org/10.1109/SILCON59133.2023.10404832.

[15] F. A. Villarroel *et al*., "Stable Shortest Horizon FCS-MPC Output Voltage Control in Non-Minimum Phase Boost-Type Converters Based on Input-State Linearization," *IEEE Transactions on Energy Conversion*, vol. 36, no. 2, pp. 1378-1391, 2021, https://doi.org/10.1109/TEC.2021.3055733.

[16] Y. Li, T. Dragičević, S. Sahoo, Y. Zhang and F. Blaabjerg, "An Improved Model Predictive Control for DC-DC Boost Converter," *2022 IEEE 13th International Symposium on Power Electronics for Distributed Generation Systems (PEDG)*, pp. 1-6, 2022, https://doi.org/10.1109/PEDG54999.2022.9923104.

[17] S. T. Bahar and R. G. Omar, "Permanent Magnet Synchronous Motor Torque Ripple Reduction Using Predictive Torque Control," *Journal of Engineering and Sustainable Development*, vol. 27, no. 3, pp. 394-406, 2023, https://doi.org/10.31272/jeasd.27.3.9.

[18] M. Almaged, S. I. Khather, and A. I. Abdulla, "Design of a discrete PID controller based on identification data for a SimScape buck boost converter model," *International Journal of Power Electronics and Drive System (IJPEDS)*, vol. 10, no. 4, pp. 1797-1805, 2019, http://doi.org/10.11591/ijpeds.v10.i4.pp1797-1805.

[19] S. Pareek, M. Kishnani and R. Gupta, "Optimal tuning Of PID controller using Meta heuristic algorithms," *2014 International Conference on Advances in Engineering & Technology Research (ICAETR - 2014)*, pp. 1-5, 2014, https://doi.org/10.1109/ICAETR.2014.7012816.

[20] S. T. Bahar and R. A. Abd-Alhmeed, "Reduce-Complexity of Predictive Current Control for a 3-Phase Voltage Source Inverter," *Journal of Techniques*, vol. 7, no. 3, pp. 16-25, 2025, https://doi.org/10.51173/jt.v7i3.2621.

[21] R. La'biran and M. Kristiawan, "Optimization of Association Rule Using Ant Colony Optimization (ACO) Approach," *Wasit Journal of Computer and Mathematics Science*, vol. 2, no. 3, pp. 100-107, 2023, https://doi.org/10.31185/wjcms.190.

[22] U. Khaleeq uz Zaman, K. Naveed and A. A. Kumar, "Tuning of PID Controller Using Whale Optimization Algorithm for Different Systems," *2021 International Conference on Digital Futures and Transformative Technologies (ICoDT2)*, pp. 1-5, 2021, https://doi.org/10.1109/ICoDT252288.2021.9441526.

[23] X. Wu, S. Zhang, W. Xiao and Y. Yin, "The Exploration/Exploitation Tradeoff in Whale Optimization Algorithm," *IEEE Access*, vol. 7, pp. 125919-125928, 2019, https://doi.org/10.1109/ACCESS.2019.2938857.

[24] B. E. Demir, "An Optimized PID Controller Design for BLDC Motor Using Nature-Inspired Algorithms," *Black Sea Journal of Engineering and Science*, vol. 7, no. 6, pp. 1177-1186, 2024, https://doi.org/10.34248/bsengineering.1539753.

[25] A. Mamizadeh, N. Genc and R. Rajabioun, "Optimal Tuning of PI Controller for Boost DC-DC Converters Based on Cuckoo Optimization Algorithm," *2018 7th International Conference on Renewable Energy Research and Applications (ICRERA)*, pp. 677-680, 2018, https://doi.org/10.1109/ICRERA.2018.8566883.

[26] M. Irshad, N. K. Vemula, R. Devarapalli, G. V. N. Kumar, and Ł. Knypiński, "An optimized integral performance criterion based commercial PID controller design for boost converter," *Journal of Electrical Engineering*, vol. 75, no. 4, pp. 258-267, 2024, https://doi.org/10.2478/jee-2024-0032.

[27] S. K. Pandey, S. L. Patil, U. M. Chaskar and S. B. Phadke, "State and Disturbance Observer-Based Integral Sliding Mode Controlled Boost DC–DC Converters," *IEEE Transactions on Circuits and Systems II: Express Briefs*, vol. 66, no. 9, pp. 1567-1571, 2019, https://doi.org/10.1109/TCSII.2018.2888570.

[28] M. Jeong and J. Biela, "Dynamic Operation of Buck-Boost DC-DC Converters over Wide Operating Ranges with Switching Based Model Predictive Control (MPC)," *2021 23rd European Conference on*

Power Electronics and Applications (EPE'21 ECCE Europe), pp. P.1-P.10, 2021, https://doi.org/10.23919/EPE21ECCEEurope50061.2021.9570537.

[29] A. Viswambharan, R. Errouissi, M. Debouza and H. Shareef, "Experimental Verification of Disturbance Observer-Based Backstepping Control for DC–DC Boost Converter," *IEEE Transactions on Circuits and Systems I: Regular Papers*, vol. 70, no. 12, pp. 5520-5533, 2023, https://doi.org/10.1109/TCSI.2023.3318970.

[30] T. Kobaku, R. Jeyasenthil, S. Sahoo, R. Ramchand and T. Dragicevic, "Quantitative Feedback Design-Based Robust PID Control of Voltage Mode Controlled DC-DC Boost Converter," *IEEE Transactions on Circuits and Systems II: Express Briefs*, vol. 68, no. 1, pp. 286-290, 2021, https://doi.org/10.1109/TCSII.2020.2988319.

[31] H. K. Khleaf, A. K. Nahar, and A. S. Jabbar, "Intelligent control of DC-DC converter based on PID-neural network," *International Journal of Power Electronics and Drive System (IJPEDS)*, vol. 10, no. 4, pp. 2254-2262, 2019, http://doi.org/10.11591/ijpeds.v10.i4.pp2254-2262.

[32] D. Guiza, D. Ounnas, S. Youcef, and A. Bouden, "PID based on a single artificial neural network algorithm for DC-DC boost converter," *Indonesian Journal of Electrical Engineering and Computer Science (IJEECS)*, vol. 31, no. 1, pp. 160-169, 2023, http://doi.org/10.11591/ijeecs.v31.i1.pp160-169.

[33] M. Forouzesh, Y. P. Siwakoti, S. A. Gorji, F. Blaabjerg and B. Lehman, "Step-Up DC–DC Converters: A Comprehensive Review of Voltage-Boosting Techniques, Topologies, and Applications," *IEEE Transactions on Power Electronics*, vol. 32, no. 12, pp. 9143-9178, 2017, https://doi.org/10.1109/TPEL.2017.2652318.

[34] X. Geng, F. Xie, B. Zhang, D. Qiu, Y. Chen and R. Wang, "Identifying Coexisting Attractors and Quantifying Dynamics Characteristics of DC–DC Converter Based on Improved Variational Mode Decomposition and Wavelet Transform," *IEEE Transactions on Power Electronics*, vol. 38, no. 3, pp. 3928-3938, 2023, https://doi.org/10.1109/TPEL.2022.3225901.

[35] B. M. Hasaneen and A. A. Elbaset Mohammed, "Design and simulation of DC/DC boost converter," *2008 12th International Middle-East Power System Conference*, pp. 335-340, 2008, https://doi.org/10.1109/MEPCON.2008.4562340.

[36] A. Malhotra and P. Gaur, "Comparative study of dc-dc converters in solar energy systems," *2014 International Conference on Advances in Computing, Communications and Informatics (ICACCI)*, pp. 816-820, 2014, https://doi.org/10.1109/ICACCI.2014.6968374.

[37] C. Yanarateş, Z. Zhou, and A. Altan, "Investigating the impact of discretization techniques on real-time digital control of DC-DC boost converters: A comprehensive analysis," *Heliyon*, vol. 10, no. 20, p. e39591, 2024, https://doi.org/10.1016/j.heliyon.2024.e39591.

[38] C. Gong, J. Lin, D. Huang and Z. Wang, "ADRC & MPC Based Control Strategy of Bidirectional Buck-Boost Converter in Distributed Energy Storage Systems," *2021 6th International Conference on Power and Renewable Energy (ICPRE)*, pp. 73-79, 2021, https://doi.org/10.1109/ICPRE52634.2021.9635464.

[39] J. Yang, H. Cui, S. Li and A. Zolotas, "Optimized Active Disturbance Rejection Control for DC-DC Buck Converters With Uncertainties Using a Reduced-Order GPI Observer," *IEEE Transactions on Circuits and Systems I: Regular Papers*, vol. 65, no. 2, pp. 832-841, 2018, https://doi.org/10.1109/TCSI.2017.2725386.

[40] S. Zhuo, A. Gaillard, D. Paire and F. Gao, "High-Order ESO-Based Voltage Control for High-Gain DC-DC Floating Interleaved Boost Converter with Time-Varying Disturbance," *2019 IEEE Transportation Electrification Conference and Expo (ITEC)*, pp. 1-6, 2019, https://doi.org/10.1109/ITEC.2019.8790514.

[41] Y. Yu and X. Hu, "Active Disturbance Rejection Control Strategy for Grid-Connected Photovoltaic Inverter Based on Virtual Synchronous Generator," *IEEE Access*, vol. 7, pp. 17328-17336, 2019, https://doi.org/10.1109/ACCESS.2019.2894786.